Supplementary information

Establishing synthesis-structure-property relationships for enhanced and reproducible MgAgSb thermoelectric properties

Amandine Duparchy [1,2], Leo Millerand [1,2], Julia Camut [1], Silvana Tumminello [1], Hasbuna Kamila[1], Radhika Deshpande[1], Aidan Cowley [2], Eckhard Mueller [1,3], Johannes de Boor [1,4]

[1] Institute of Materials Research, German Aerospace Center (DLR), Cologne, Germany

[2] European Astronaut Center, European Space Agency (ESA), Cologne, Germany

[3] Institute of Inorganic and Analytical Chemistry, Justus Liebig University Giessen, Giessen, Germany

[4] Institute of Technology for Nanostructures (NST), Faculty of Engineering and CENIDE, University of Duisburg-Essen, Duisburg, Germany

As shown in Table S1, the chosen reference ($MgAg_{0.97}Sb_{0.995}$) is made of >99 % of the matrix and <1 % of impurity (Sb), comparable to sample 8-p reported in I. Rodriguez-Barber's paper [1]. After Rietveld Refinement the weighted profile Rfactor (Rwp) is up to 13 while the Goodness of fit is equal to 3 [2].

Table S1: Sum up of Rietveld refinement of the reference sample c-20-13

R-Values			
R-expected (Rexp)	*R-weigthed pattern (Rwp)*	*R-pattern (Rp)*	*Goodness of fit (GOF)*
4.43	*13.26*	*10.40*	*2.99*
Background corrected factor			
Rexp`: 5.91	*Rwp`* : 17.69	*Rp`*: 15.16	*DW :* 0.59
Quantitative Analysis – c-20-13			
Phase 1	α-MgAgSb 99.2 wt%		
Phase 2	Sb 0.8 wt%		

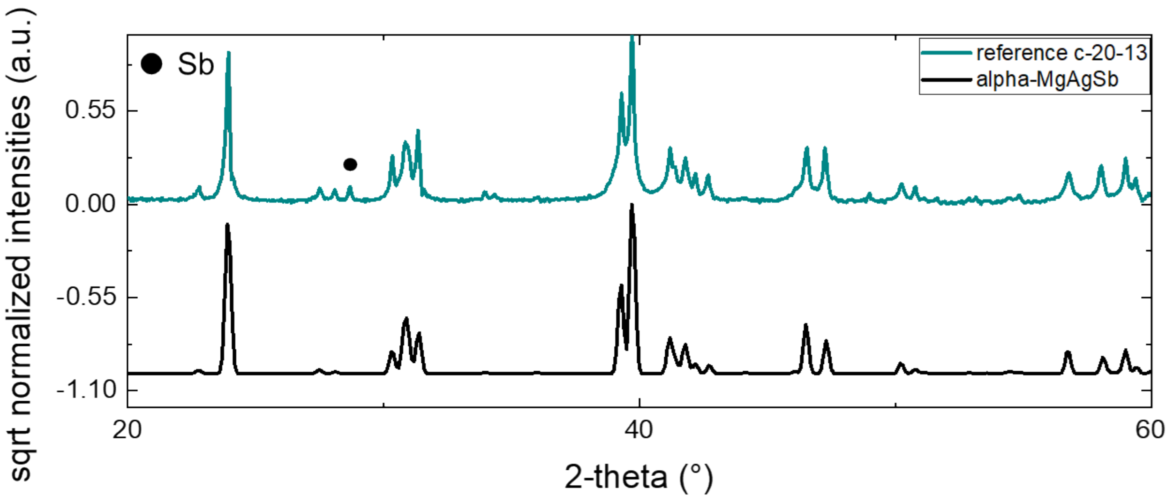

Figure S1: XRD patterns of c-20-13 (reference sample)

XRD pattern of the sintered MgAg precursor are reported in Rodriguez Barber et al. [1]. The corresponding XRD-pattern can be found in figure 3.a., p4 in section 3.4. In our case, MgAg underwent the same synthesis process as sample 8-p.

Figure S2 presents all the samples plotted on the calculated ternary diagram for Ag-Mg-Sb system at 300 °C using the EDX-SEM measurement results directly. All samples are apparently Mg-poor, in contradiction to nominal stoichiometry and observed secondary phases, presumably due to EDX systematic error.

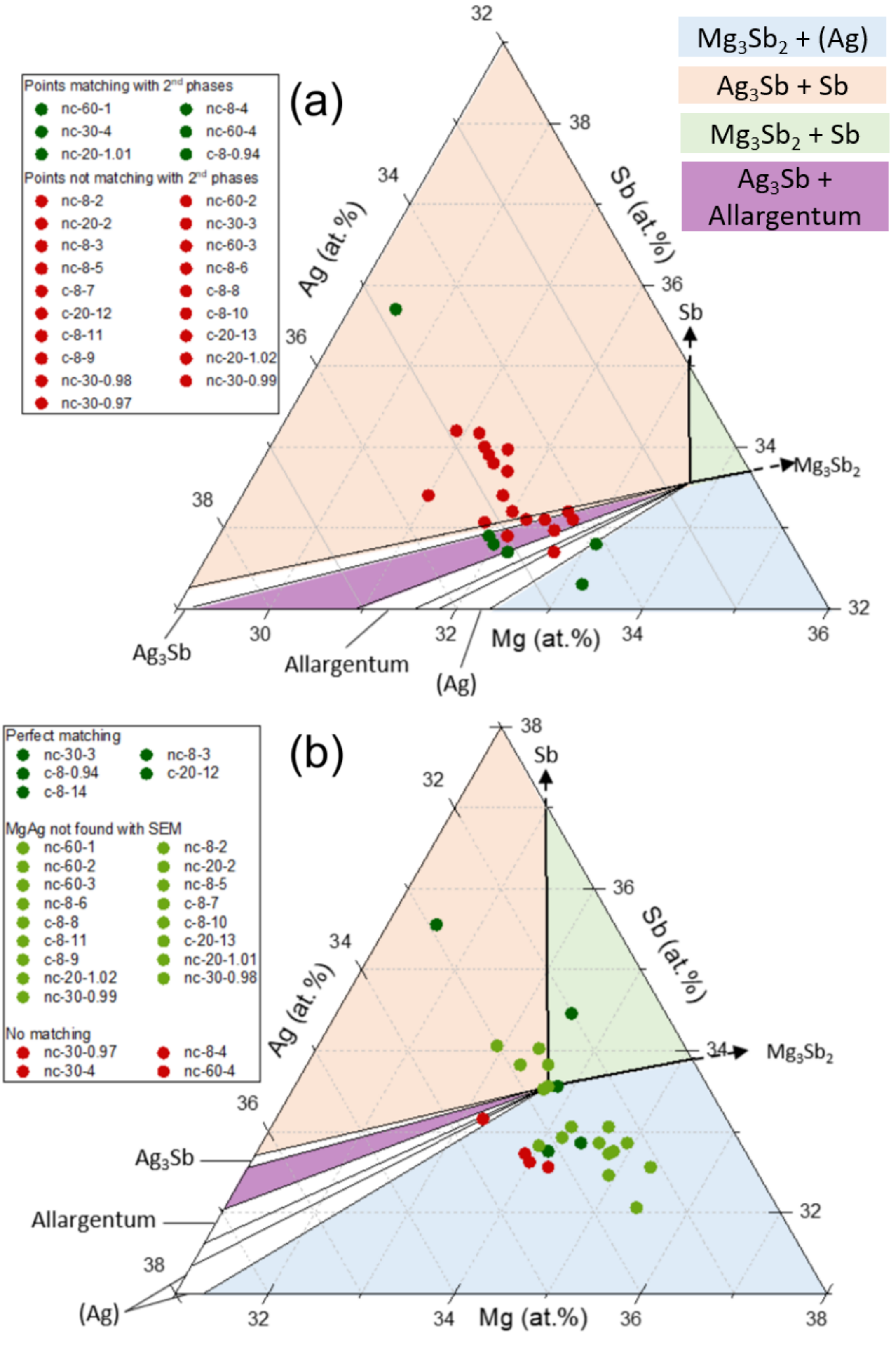

Figure S2: Ag-Mg-Sb calculated ternary diagram at 300 °C with the sample positions according to their measured effective compositions. (a) shows the position according to the EDX result, with all samples being Mg deficient region, (b) shows the *new samples position after calibration on the phase diagram. Each marker corresponds to the EDX measured averaged composition. Green indicates agreement between secondary phases determined by XRD and secondary phases expected according to the position on the phase diagram, while red indicates disagreement.*

An example for the calibration is given for sample c-8-10 in Table S2.

Table S2: Table illustrating the calibration used on the effective compositions. The measured composition of the reference and c-8-10 sample are given, as well as calibrated effective composition with calculated shift.

	Measured composition		Difference between measured and assumed composition	Calibrated composition	
	Reference	**c-8-10**	**Reference**	**Reference**	**c-8-10**
Mg (at%)	31.5	31.1	+2.2	33.7	32.9
Ag (at%)	34.8	34.6	-2.1	32.7	33.1
Sb (at%)	33.7	34.1	-0.1	[illegible]	33.7

Figure S3 gives an overview of the samples used for the study. … rder to be able to identify all the … on the ternary phase di… C.

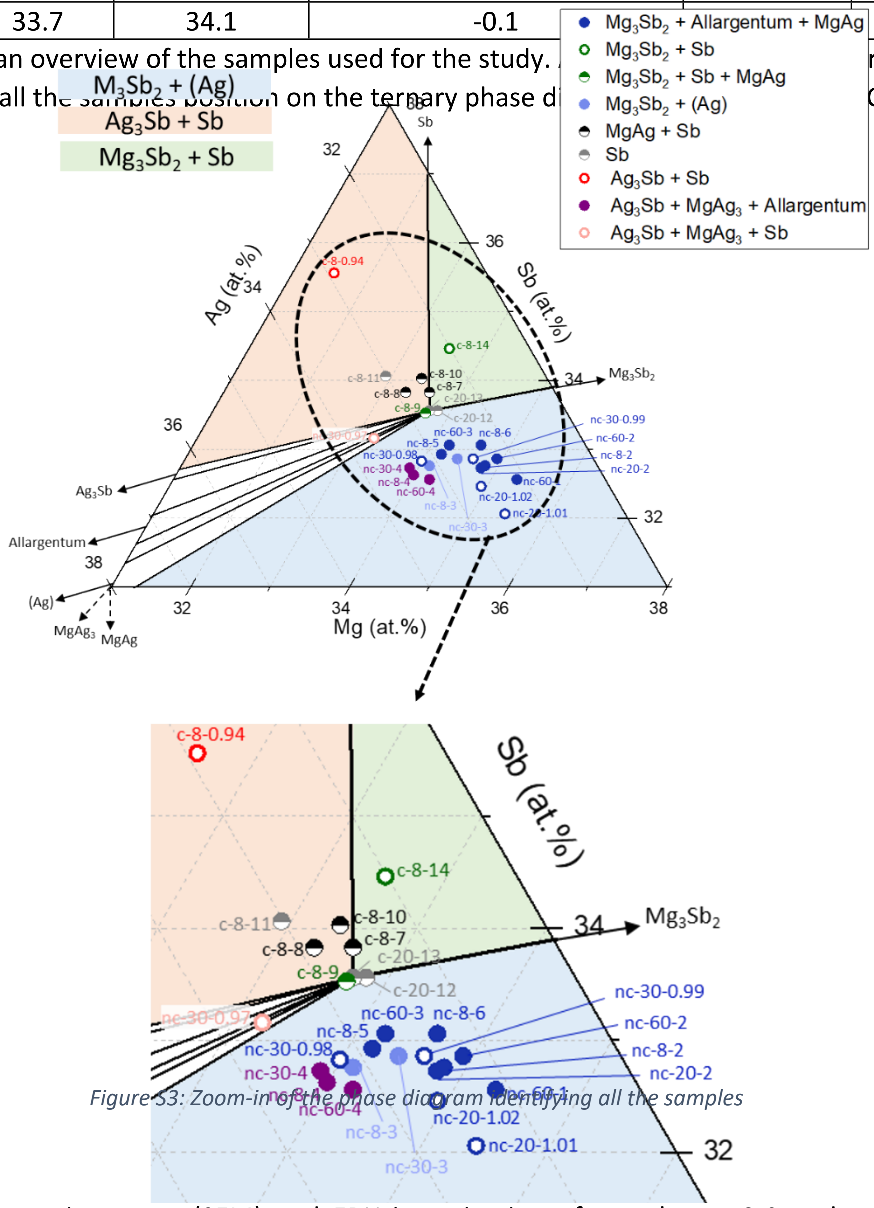

Figure S3: Zoom-in of the phase diagram identifying all the samples

Scanning electron microscope (SEM) and EDX investigation of samples nc-8-2 and c-8-9 reveal a difference in terms of size and type of the secondary phases. The nc-8-2 sample shows Mg_3Sb_2 & (Ag) as impurities while c-8-9 contains Mg_3Sb_2 & Sb as impurities. (Ag) refers to silver with some dissolved magnesium and/or antimony (2 < at. %< 5) [3].

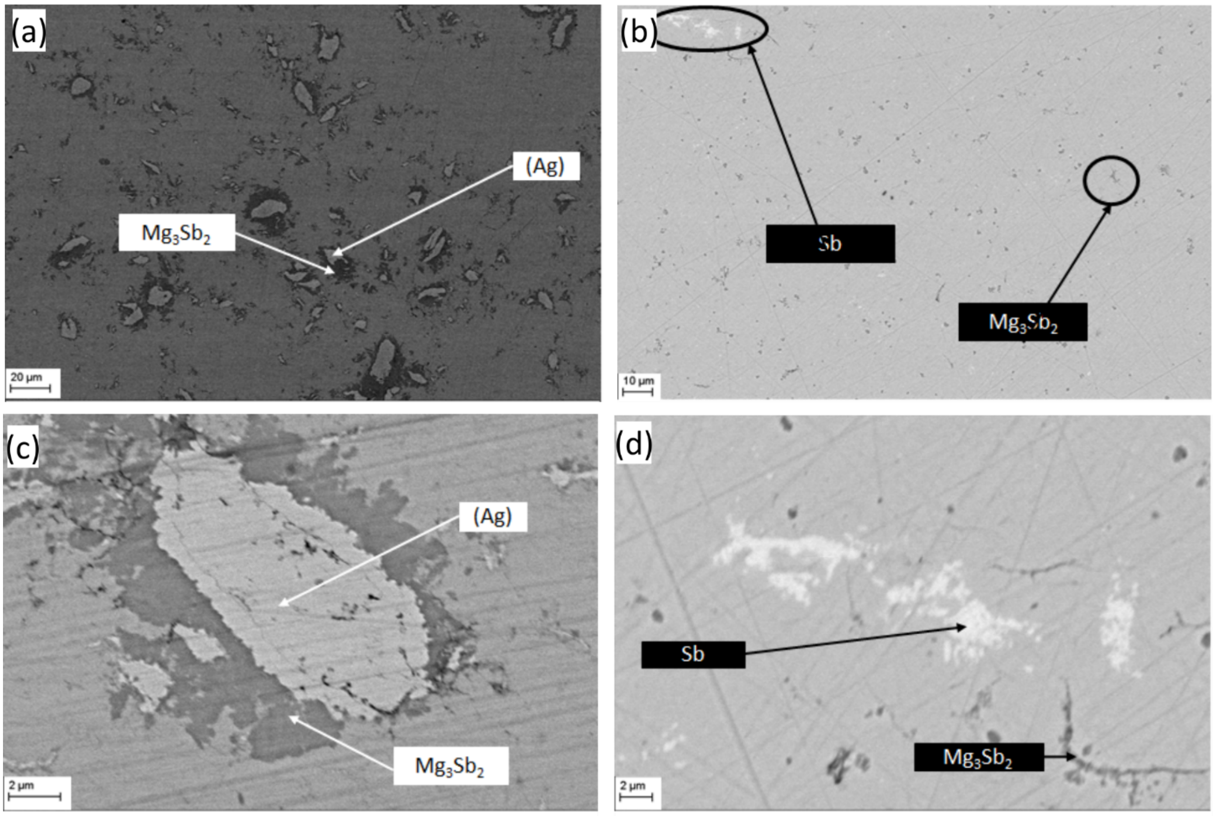

Figure S4: SEM images of (a)(c) a sample before the additional cleaning step with (Ag), the Silver rich solution and Mg_3Sb_2 as secondary phases (b)(d) a sample with the additional cleaning step with Mg_3Sb_2+ Sb as secondary phases

Table S3: EDX point analysis to confirm the assigned phases. Left part of the table corresponds to nc-8-2 sample and right part to c-8-9 sample. The composition is given in atomic percent.

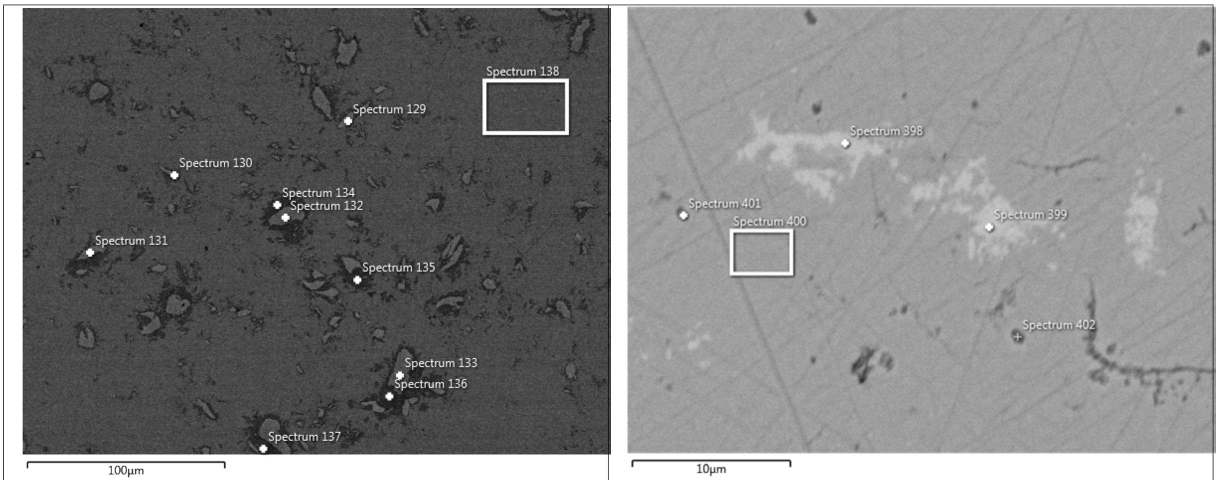

	Mg (at%)	Ag (at%)	Sb (at%)		Mg (at%)	Ag (at%)	Sb (at%)
Spectrum 133	8.05	85.99	5.96	Spectrum 401	42.20	22.51	35.29
Spectrum 134	56.32	4.59	39.09	Spectrum 398	4.49	7.65	87.86

Figure S5, S6 and S7 are plotted using cooling data.

As shown in Figure S5, the Seebeck coefficient of c-8-9 is lower than nc-8-2, decreasing along the temperature range. One can see that the Seebeck curves start to bend at the same temperature and decrease monotonously along the temperature range in parallel. Furthermore, the electrical conductivity behaves inversely to the Seebeck coefficient. The thermal conductivities for both samples are similar except at low temperature (below 400K) with a lower thermal conductivity for c-8-9 which could be due to a higher phonon scattering or higher thermal conductivity of the secondary phases. The difference in zT is mainly due to higher charge carrier concentration and mobility of c-8-9 ($n_{nc\text{-}8\text{-}2}$=4.0*10^{19} cm^{-3} / $n_{c\text{-}8\text{-}9}$=4.6*10^{19} cm^{-3} and $\mu_{nc\text{-}8\text{-}2}$= 20.9 cm^{2}V^{-1}s-1 / $\mu_{c\text{-}8\text{-}9}$= 33.7 cm^{2}V^{-1}s^{-1}) but also because of much larger differences in electrical conductivities and Seebeck coefficient. One can deduce say that the thermoelectric properties of MgAgSb are greatly influenced by the type, number and size of the secondary phases.

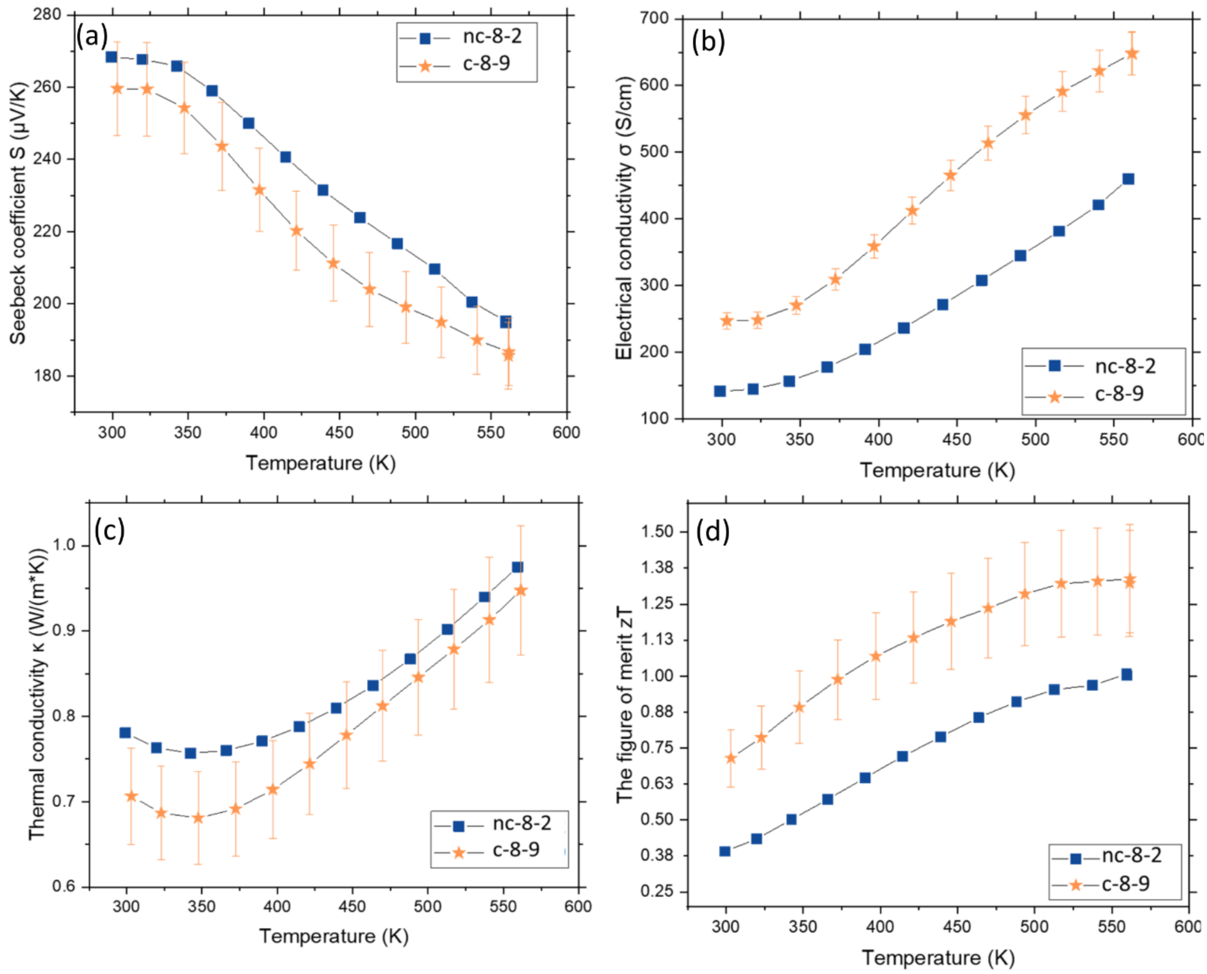

Figure S5: (a) Seebeck coefficient (b) electrical conductivity (c) thermal conductivity (d) figure of merit for the samples from nc-8-2 (before the additional cleaning step) & c-8-9 (after the additional cleaning step).

The graphs from Figure S6 are plotted to analyze the evolution and behavior of the thermoelectric properties (Seebeck coefficient, electrical conductivity, thermal conductivity and lattice thermal conductivity) of 6 batches in comparison to literature values from Liu et al. [4].

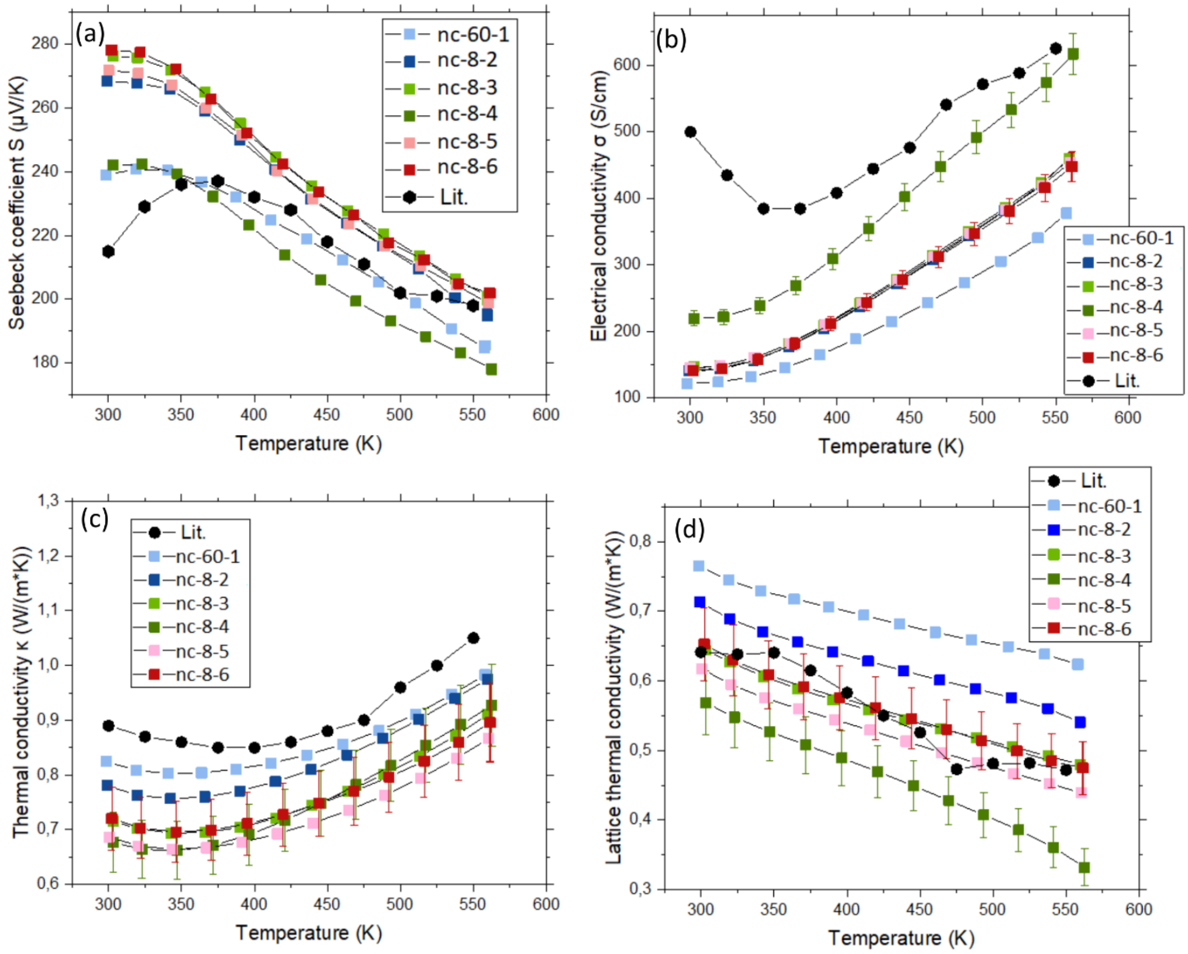

Figure S6: (a) Seebeck coefficient (b) electrical conductivity (c) Thermal conductivity (d) lattice thermal conductivity for the samples synthesized without the additional cleaning step

Reproducible and enhanced thermoelectric properties of batches 7 to 10 are depicted in Figure S7. It is clear that the curves are nearly superposed and within the same range and the literature data. c-8-9 is the best sample with the highest zT which behaves differently from the other batches at high temperature except for the lattice thermal conductivity.

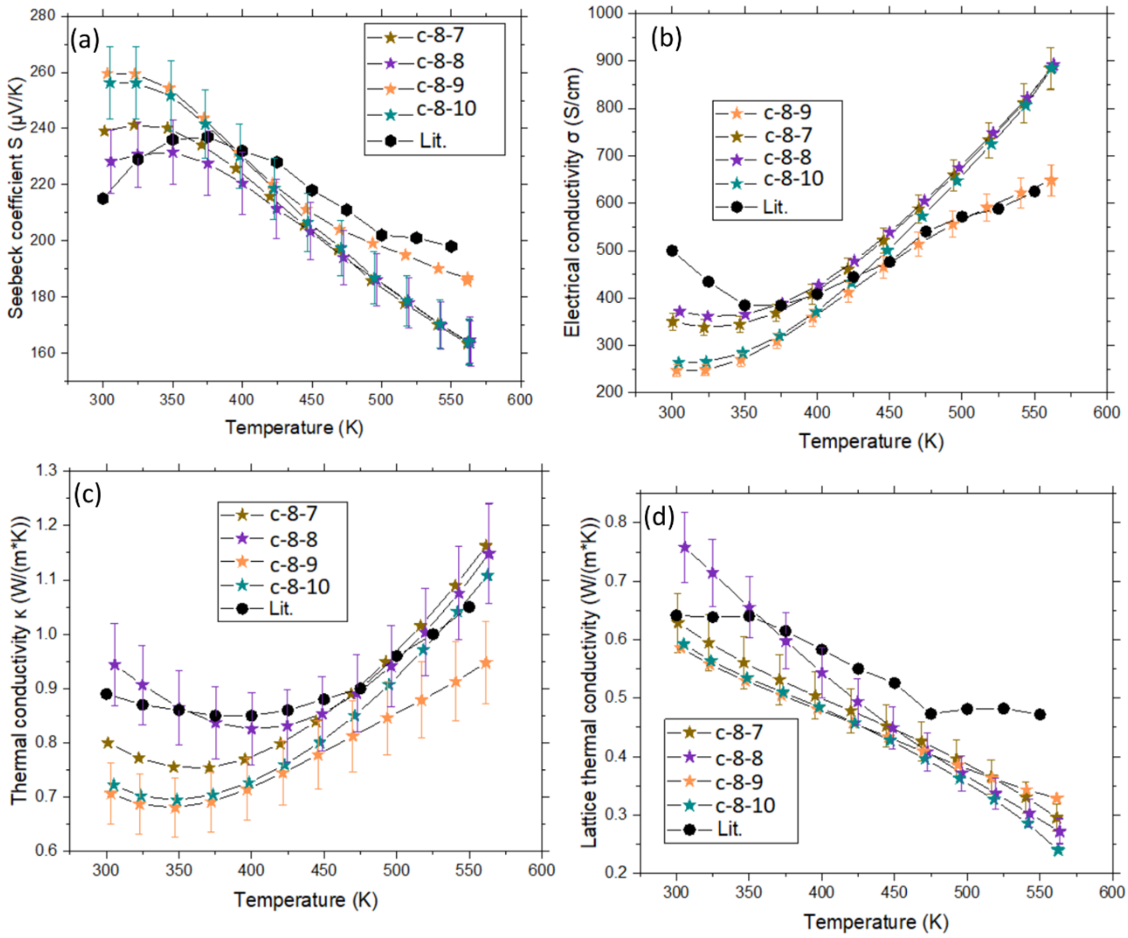

Figure S7: (a) Seebeck coefficient (b) electrical conductivity (c) Thermal conductivity (d) lattice thermal conductivity for the samples synthesized with the additional cleaning step

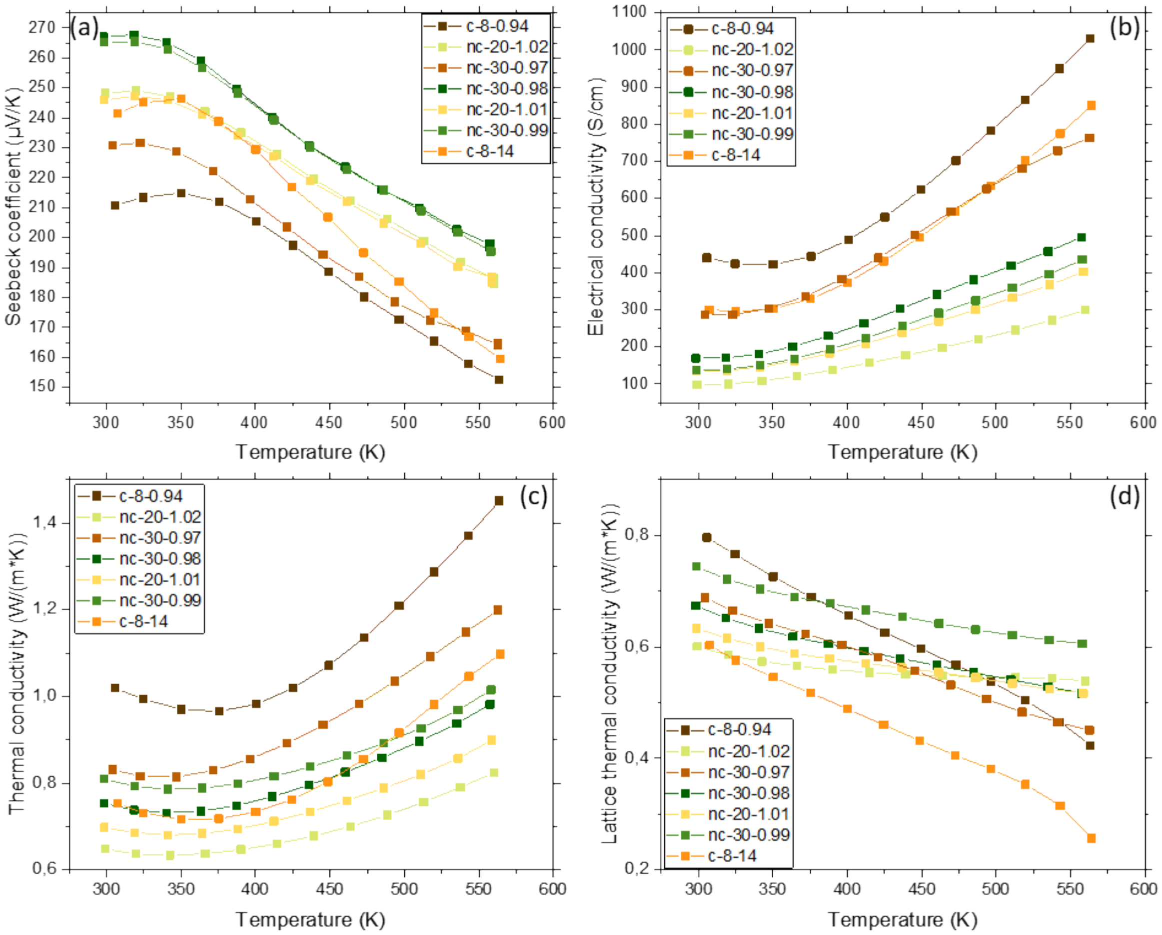

Figure S8: (a) Seebeck coefficient (b) electrical conductivity (c) Thermal conductivity (d) lattice thermal conductivity for the samples synthesized with composition variation in Mg, Ag and/or Sb.

Assuming the typical behaviour for a semiconductor with a majority carrier band and a minority carrier band a change in T_{Smax} is expected with a change in the charge carrier concentration. For the samples presented in the manuscript, the Seebeck coefficient varies between 210 and 280 µV/K. The charge carrier range is then smaller as in the case of MgAgSb doped with Lithium [5] but still shows a shift in the maximum T_{Smax}. For instance, c-8-8 has a maximum temperature at ~350 K while nc-8-6 rather at 300 K.

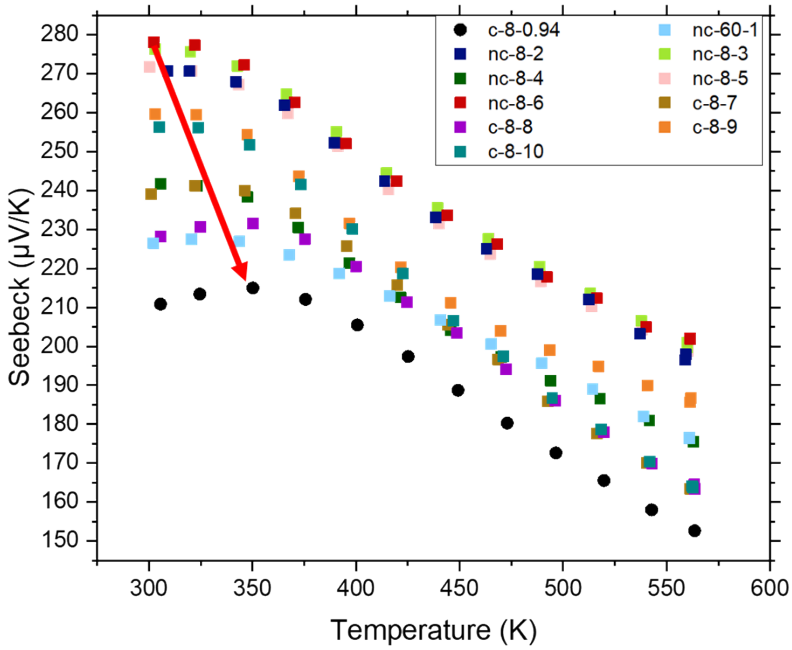

Figure S9:Compiled S(T) for representative samples discussed in the manuscript, showing an increase of $T(S_{max})$ *with decreasing* $S(T = 300\ K)$*, i.e. increasing carrier concentration.*

1. Rodriguez-Barber, I., et al., On the influence of AgMg precursor formation on MgAgSb microstructure and thermoelectric properties. Journal of Alloys and Compounds, 2021. 860.
2. Toby, B.H., R factors in Rietveld analysis: How good is good enough? Powder Diffraction, 2012. 21(1): p. 67-70.
3. Raynor, F.a., The system silver-magnesium-antimony, with reference to the theory of alloy formation. Proc. R. Soc. London. Ser. A. Math. Phys. Sci., 1950. 203(1072): p. 132-147.
4. Liu, Z., et al., Effects of antimony content in MgAg0.97Sbx on output power and energy conversion efficiency. Acta Materialia, 2016. 102: p. 17-23.
5. Liu, Z., et al., Lithium Doping to Enhance Thermoelectric Performance of MgAgSb with Weak Electron-Phonon Coupling. Advanced Energy Materials, 2016. 6(7).